

Experimental and numerical analysis of interfacial fracture in piezoelectric composites

RUIXIANG BAI*, LIANG WANG, ZHENKUN LEI, HAORAN CHEN

State Key Laboratory of Structural Analysis for Industrial Equipment, Dalian University of Technology, Dalian 116024, P.R. China

In this paper, piezoelectric composite specimens with epoxy resin adhesive for fixed-ratio mixed-mode (FRMM) fracture tests with photoelasticity analysis were performed. The deformation and strain field are obtained by digital image correlation (DIC) technologies, and the beam theory is used to calculate the critical fracture energies for piezoelectric composites. The values of SERR were calculated using the Virtual Crack Closure Technique and the traction-separation law for VCCT and CZM approaches respectively. Good agreement of the load-displacement response was obtained between the FEA and experimental results when using CZM approach. On the other hand, although the VCCT approach cannot provide precise simulation of the crack initiation, it can be considered as an efficient alternative in modelling the crack propagation phase. Our study demonstrates the digital photoelastic FRMM test is simple and validated for piezoelectric composite and the CZM can well characterize the interface debonding fracture of piezoelectric composite materials with a weak bonding interface.

(Received November 2, 2011; accepted November 23, 2011)

Keywords: Piezoelectric composite, Fracture toughness, Finite element analysis, Debonding, Photoelasticity

1. Introduction

Interfacial fracture in adhesively bonded piezoelectric laminated structures presents an important concern in multilayer devices, especially under mechanical loading, during which interfacial debonding is often observed because of stress concentration due to the mismatch of material, leading to failure of these devices. The problems of an interface crack between two different piezoelectric materials or between piezoelectric materials and elastic substrates have been studied by many researchers [1-3].

An experimental technique was developed by Du et al. to address this issue especially [4]. The technique involves using piezoelectric actuators to apply cyclic loading to an adhesively bonded specimen with a polymer-aluminum interfacial crack. The PZT thin films were deposited by sputtering different metal or ceramic layers onto a single-crystal silicon substrate, and a series of sandwiched-cantilever type specimens were tested in the experiment by Shang et al. [5]. These experimental results can provide the total energy or fracture loads of these specimens, but can not be used to characterize the mixed mode of the piezoelectric composite structures. While various specimen geometries encompassing all of the different modes of failure have been proposed, only some success has been achieved with regard to the standardization of such test methods [6-8]. However, specialized methodologies for quantifying adhesive fracture toughness for piezoelectric structures are limited due to unique experimental challenges [9], as piezoelectric ceramic materials are brittle and weak tensile fracture strength, and also extremely difficult to machine into test geometries specified by ASTM, JIS, and ISO test standards. Based on the work of Hashemi et al. [10,11], we

find an effective test method for the fracture toughness of piezoelectric/composite that is the fixed-ratio mixed-mode (FRMM) test, as shown in Fig. 1.

Photoelasticity and digital image correlation (DIC) technologies have been extensively used to study the fracture of homogeneous materials [12]. A photoelasticity investigation of bimaterial interfaces was first performed on isotropic/isotropic bimaterials. Gdoutos and Papakaliatakis were the first to perform such a study on the static behavior of an interface crack in an isotropic/isotropic bimaterials [13]. They demonstrated that the photoelastic method was applicable to this problem and presented the mathematical and experimental methods to perform such an analysis. Lu and Chiang [14] expanded on this work and proposed two different approaches in determining the stress-intensity factors from the isochromatic fringe patterns. Ellingsen [15] et al. use transmission photoelasticity to investigate the mechanical behavior of composite/composite bimaterials and directly observe the stress distribution around the crack tip. Thus, digital photoelasticity combined with high-speed photography can be effectively used to record the full-field strain or stress data for propagating cracks, from which the necessary fracture parameters can be extracted. However, a very limited literature can be found on piezoelectric /composite interface fracture by photoelasticity and DIC method.

Debonding of adhesively bonded joints and delamination of composite materials are major concerns in aero structures. The direct way to study these problems is to use fracture mechanics in conjunction with the FE method. Among fracture parameters, the strain energy release rate is used increasingly in conjunction with LEFM. As to the energy-based criterion, the virtual crack

closure technique (VCCT) is a powerful tool to compute SERR by using finite element analysis. Some applications of VCCT to study the crack growth can be found in [16]. Similarly to the VCCT, the energy release rate and the critical cohesive strength are also key parameters in a cohesive zone model (CZM), but in the CZM, fracture is modeled by the cohesive laws instead of the stiff springs [17]. The CZM has been widely used to describe fracture and failure in metals, ceramics, polymers, and composite materials, and has successfully interpreted a variety of problems, such as crack tip plasticity and creep, crazing in polymers, and adhesively bonded joints and interface cracking in bimetals [18,19]. Therefore, progressive failure of the adhesive layer can be described using a CZM in which the failure behavior is expressed by a traction–separation law. The traction–separation law is defined by three cohesive parameters: the critical cohesive strength, the initial stiffness and the fracture toughness. The fracture toughness can be determined by experiments, but there are no standard methods to obtain the critical cohesive strength and the initial stiffness. In most cases, these parameters are determined iteratively by adjusting the simulation results to the experimental results [20,21].

Following the introduction, Section 2 describes the material system, the FRMM experimental procedure, DIC technologies and the data reduction schemes which used to calculate the critical fracture energy release rates of piezoelectric composite specimens. The numerical analysis model is summarized in Section 3. Comparisons between numerical and experimental results, and also the effect of some interface parameters on the load–displacement response are all given in Section 4. Finally a brief summary and conclusions is presented in Section 5.

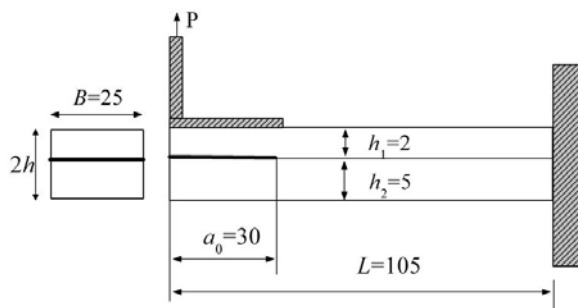


Fig. 1. Schematic representation of the FRMM test and geometry dimensions.

2. Experimental works

2.1 Material

The piezoelectric ceramics (PZT-5) employed was produced by Baoding HongSheng Acoustics Electron Apparatus Co., Ltd. (Baoding, China), elastic properties were measured experimentally in three point bending tests ($E=60\text{GPa}$, $\nu=0.3$). The carbon-fiber epoxy resin composite (T300/QY8911) with 0.125 mm ply thickness were employed, whose mechanical properties are

presented in Table 1. The epoxy resin adhesive was employed for the experiment which was manufactured by elementary mechanics experiment center of Dalian University of Technology, whose elastic properties were measured experimentally in bulk tests ($E = 1\text{GPa}$, $\nu = 0.3$).

Table 1. T300/QY8911 elastic properties.

| | | |
|-------------------------|-------------------------|-----------------|
| $E_{11}=126\text{GPa}$ | $G_{12}=4.47\text{GPa}$ | $\nu_{12}=0.33$ |
| $E_{22}=10.7\text{GPa}$ | $G_{13}=4.47\text{GPa}$ | $\nu_{13}=0.33$ |
| $E_{33}=10.7\text{GPa}$ | $G_{23}=3.57\text{GPa}$ | $\nu_{23}=0.38$ |

2.2 Specimen

Fig. 1 shows the geometry and dimensions of the FRMM specimens. In order to provide crack growth stability, the initial crack length was considered to be equal to 60% of the half-length of the specimen. Teflon tapes are placed on the edges, with silicon grease applied on them, for easy removal after curing, to form the edge cracks. The epoxy resin adhesive is applied on the surfaces to be bonded, light pressure is applied, and the specimen is allowed to set at the same elevated temperature conditions for about 24 h. And the bonding thickness is about 0.2 mm. After curing, the Teflon tape is easily removed, forming the interface edge crack. Two specimens in Table 2 are used in this test. A face of the specimen is speckled with black and white color sprays in order to create a random speckle pattern on the surface, as indicated in Fig. 2. During the test, the Canon SX100 was used to record the images with a resolution of 1600×1200 pixels which facing perpendicularly to the specimen surface. The black and white painting can also provide good optical contrast for monitoring crack growth and may help minimize the reading errors made when measuring crack length by visual inspection during the test. The interval of time between each image is set at 0.25 seconds. Measurements of displacements on the surface of the specimens and calculations of strain fields are performed from the image processing program whose principle is based on the following DIC method.

Table 2. Adhesive and stacking sequences of the specimens.

| Specimen | Adhesive | stacking sequences | Pre-crack length (mm) |
|----------|-------------|--------------------|-----------------------|
| A | Epoxy resin | $[0]_{16}$ | 30 |
| B | Epoxy resin | $[0_2/90_2]_{25}$ | 30 |



Fig. 2. Piezoelectric composite specimen and the applied speckle pattern.

2.3 Test conditions

Specimens were tested using an INSTRON3345 (Norwood, MA) testing machine at room temperature under displacement control. Fig. 3 shows the experimental setup. Running in load-control mode and using a 5-kN reversible load transducer, the specimens were loaded at a displacement rate of 0.2 mm/min. The load–displacement ($P-\Delta$) curve was registered during the test. Prior to testing, a graph paper was placed against the specimen surface and its image was captured to calibrate the image distances to real distances. The experimental values of $P-\Delta-a$ as a function of time were obtained. The time of each $P-\Delta$ data point was calculated from the applied displacement. The time for each value of a is the one at which the corresponding photo was taken.

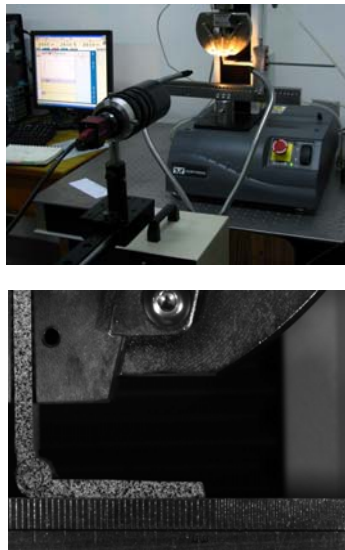


Fig. 3. Experimental devices and calibration of photoelastic test region.

2.4 Principles of digital image correlation

A digital image is essentially a two-dimensional array of intensity values which can be discretized into small subsets. Image correlation works by matching small square subsets of an undeformed image to locations in the image of the surface after deformation, as shown in Fig. 4. For this technique to work well a grey scale random pattern is needed on the surface of the specimen. To recognize this pattern mathematically, the intensity of each pixel in the reference and deformed images can be traced and the displacement vector can be determined. Assume that a point A in the reference image with a $x-y$ coordinate system is mapped into point \bar{A} in deformed image with a $\bar{x}-\bar{y}$ coordinate system. The mapping can be given as:

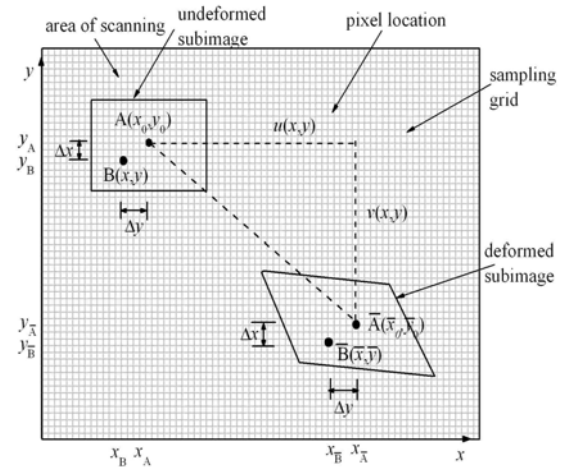


Fig. 4. Corresponding relation of deformed and undeformed subimages.

$$\begin{aligned} \bar{x} &= x + u(x, y) \\ \bar{y} &= y + v(x, y) \end{aligned} \tag{1}$$

To find the displacement fields, the vertical v , and horizontal u , displacements can be approximated using the first order Taylor series around a point $A(x_0, y_0)$ as:

$$\begin{aligned} \bar{x} &= x_0 + u + \frac{\partial u}{\partial x} \Delta x + \frac{\partial u}{\partial y} \Delta y \\ \bar{y} &= y_0 + v + \frac{\partial v}{\partial x} \Delta x + \frac{\partial v}{\partial y} \Delta y \end{aligned} \tag{2}$$

where $\Delta x = x - x_0$ and $\Delta y = y - y_0$.

Depending on the use of a first order approximation, there are six parameters $u, v, \frac{\partial u}{\partial x}, \frac{\partial v}{\partial x}, \frac{\partial u}{\partial y}$ and $\frac{\partial v}{\partial y}$,

which are available and can be found correlation between the two images. By trial and error, an iterative process is performed to estimate these parameters of the displacement and strain components for each subset until the optimal matching between the intensity values at each point in the undeformed and deformed regions is achieved.

The correlation coefficient Q is formulated to describe the similarity degree between as follows:

$$Q\left(u, v, \frac{\partial u}{\partial x}, \frac{\partial v}{\partial x}, \frac{\partial u}{\partial y}, \frac{\partial v}{\partial y}\right) = 1 - \frac{\sum G(x, y)F(x', y')}{\sqrt{\sum G^2(x, y)}\sqrt{F^2(x', y')}} \quad (3)$$

where $G(x, y)$ and $F(x', y')$ are the grey scale light intensities corresponding to all the points in the subset, here, correlation coefficient Q plays a key role as a quantitative measure of the accuracy of the match where $Q = 0$ represents a perfect match and $Q = 1$ is a complete mismatch.

A successful image correlation algorithm will provide a displacement map that is as detailed as possible (high spatial resolution) and as accurate as possible, so that it can be differentiated to give a strain map. Any displacement on the surface being imaged is digitized by the camera into a pixel array. Then the linearized strain components are given by:

$$\varepsilon_x = \frac{du}{dx}, \varepsilon_y = \frac{dv}{dy}, \varepsilon_{xy} = \frac{du}{dy}, \varepsilon_{yx} = \frac{dv}{dx} \quad (4)$$

Where (u, v) and $(u+du, v+dv)$ are two surface displacement vectors located (dx, dy) apart. And, if a detailed strain map is to be obtained, then subpixel displacement resolution and accuracy are necessary. Based on the theory above, a photoelastic digital image software by VC++6.0 is used here to reduce the photoelastic data.

2.5 Data reduction schemes

After the deductions of Hashemi et al. [10,11], it is possible to determine the energy release rate G of a delamination specimen based on the applied moments at the end of a crack, as shown in Fig. 5. The zoom of the crack tip in the figure shows the applied loads and moments, which are uniform in the width direction. The upper beam is loaded with a moment M_1 , an axial force N_1 and a shear force Q_1 , while the lower beam is loaded with a moment M_2 , an axial force N_2 and a shear force Q_2 . However, in this case the axial forces are zero and, in general, the effect of the shear forces is neglected. Then, according to the beam theory, the

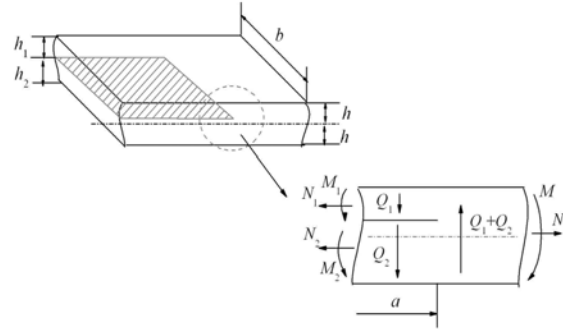


Fig. 5. Delamination geometry and crack tip loaded with axial and shear forces and moments.

mode I and mode II components of the energy release rate for the FRMM test when only moments are applied can be calculated as follows:

$$G_I = \frac{6P^2(a + \chi_I h_1)}{bE_{11}h_1^3 \left(1 + \left(\frac{h_1}{h_2}\right)^3\right)} \quad (5)$$

$$G_{II} = \frac{18P^2(a + \chi_{II} h_1)^2 \left(\frac{h_1}{h_2}\right)^4}{bE_{11}h_1^3 \left(1 + \frac{h_1}{h_2}\right)^2 \left(1 + \left(\frac{h_1}{h_2}\right)^3\right)}$$

where the parameters χ_I and χ_{II} are the correction crack length factors to take into account that the deflection of the specimen beams is not zero at the crack tip. The expressions for χ_I and χ_{II} can be found elsewhere [25].

3. Numerical simulations

Finite element simulation is performed to analyze the failure mechanism behavior of piezoelectric composite laminates bonded interface in the FRMM configuration (see Fig. 1) using a commercial finite element code ABAQUS. Based on two method, virtual crack closure technique(VCCCT) and cohesive zone model(CZM), the FRMM specimen containing the piezoelectric composite laminates bonded interface is simulated using eight node, reduced integration, continuum shell elements (SC8R) for piezoelectric composite specimens. A single zero thickness layer of cohesive element (COH3D8) through the thickness of adhesive is for the cohesive zone model. Then the damage cohesive model [23] is implemented in finite element (FE) modeling of the piezoelectric composite laminates specimens containing epoxy resin adhesive bonded interfaces. In addition, the contact is defined between the open faces of the pre-existing crack to avoid crack surface penetrations.

4. Results and discussions

The length of 1 mm corresponds to about 21 pixels in the images obtained by digital camera. Once the deformations of a speckle pattern applied to the specimen have been measured, the displacement distribution in the specimen can be calculated. In Fig. 6 the displacement results obtained with the DIC technique are compared with the finite element simulation results for specimen A. The pictures were taken immediately prior to failure of the specimen at a load of P_{max} . A quite satisfactory agreement between numerical and experimental results is noted either if the experimental displacement field is a little noisier than the numerical one. It is clearly shown that the horizontal displacement fields are noisy comparing with vertical displacement fields. The characteristic form of the displacement field around the crack is perhaps most evident in the measured vertical displacement vectors local to the crack used to determine the instantaneous stress or strain values. In addition, the asymmetrical displacement distributions are observed to reflect the mixed-mode loading.

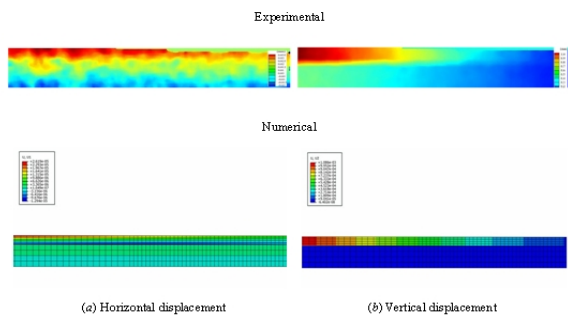


Fig. 6. Comparison between results of displacement fields by the DIC and FE simulations.

Strain maps around the crack tip are obtained from the experiments by the DIC shown in Fig. 7. As commented with regard to displacement fields, the strain fields of ϵ_x and ϵ_{xy} are quite diffuse as a result of numerical differentiation of displacement fields. So we can not get useful results around the crack tip from strain ϵ_x and ϵ_{xy} . Maybe the image correlation would collect more points in the vicinity of the crack at a higher resolution, it would capture the strain ϵ_x and ϵ_{xy} around the crack tip more clearly. Nevertheless, there is preferential ϵ_y with the direction of growth in the bonding line shown in Fig. 7. The vertical strain ϵ_y in adhesive interface changes with applied load, we can see the change is dramatic around the crack tip, and the reason is the effect of local around crack tip. Using these maps as a guide, inspection of the strain field ϵ_y during debonding shows that the high-strain region is in fact associated with debonding procession of the piezoelectric composite.

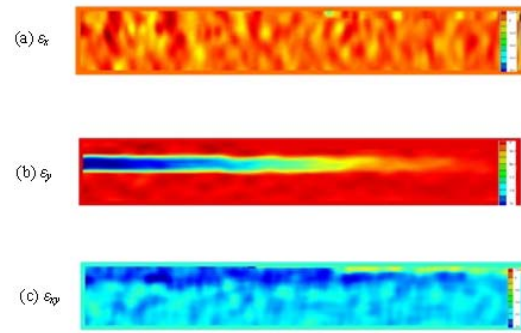


Fig. 7. Comparison between results of strain fields by DIC.

Then, the mode I fracture energy values calculated by Eq.(5) were calculated to be 6.35 ± 0.7 N/m and 7.9 ± 0.8 N/m for the A and B specimens, the mode II critical fracture energy components were calculated to be 0.45 ± 0.1 N/m and 0.4 ± 0.1 N/m for the A and B specimens, respectively. The purely adhesive failure and failure from an internal flaw of adhesives were not found in this study. We observed only failures that were initiated and propagated at the piezoelectric ceramic-adhesive interface for epoxy resin adhesive specimen, the strongest interface bond occurred at the adhesive-composite interface. Thus, we expect all failures to occur at the weaker adhesive piezoelectric ceramic interface which resulted in lower fracture energy values. By comparing the fracture energies of typical metal or other composite materials adhesive interface, the fracture energy of this piezoelectric composite interface is also quite low. It is thus confirmed that the examined piezoelectric composite interface is weakly bonded and its fracture process is characterized as brittle.

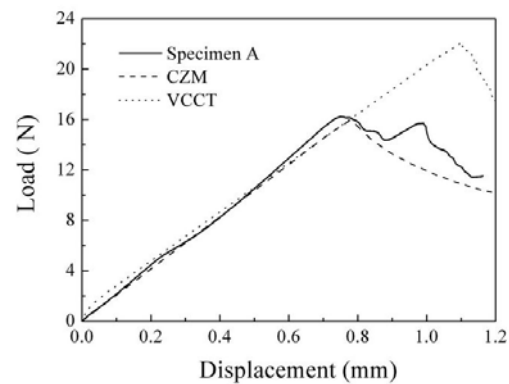


Fig. 8. FEM and experimental Load - displacement response of specimen A.

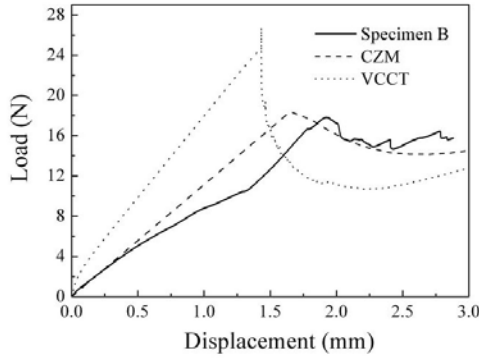


Fig. 9. FEM and experimental Load - displacement response of specimen B.

Except the critical energy release rate, the key parameters of the CZM include cohesive strength and the interface stiffness, respectively. A number of sets of these parameters are utilized in the simulation to best match the experimental results. Based on tensile test of epoxy resin adhesive and preliminary calculations, a reasonable value for the cohesive strength, σ_{ic} , is found to be 1MPa. The load-displacement curves of the finite element analysis by CZM were displayed and compared to experimental results as shown in Fig. 8 and Fig. 9, for comparison the simulating results of the CZM, the simulation results by VCCT were also shown. The fracture behavior for piezoelectric composite of FRMM specimens in Fig.8 and Fig. 9 show that the finite element analysis with the mixed-mode cohesive zone model well describes the experimental results. According to the curves, good agreement is achieved between CZM model and experiments, the error of maximum load P_{max} are only 7.7% and 5.8%. But for VCCT method, the value of maximum load P_{max} is much higher than experiment results, the error of the maximum load prediction P_{max} is about 30%-50%.The VCCT based on linear fracture mechanics which assuming the adhesive interface is rigid, the interface stress and fracture toughness would be overestimated, as shown in Fig. 8 and Fig. 9. So the CZM method is more accurate than VCCT to piezoelectric composite in this study, but the cohesive strength needs to be calibrated from specimens based on the assumed cohesive law or as it has been measured. It also reveals that, the examined piezoelectric composite interface is weakly bonding strength, as the cohesive strength increases, the maximum load increases. In addition, from the experimental results, we can see the load P_{max} is very closed, though the stacking sequences is different, but there is a big effect on load point displacement for different stacking sequences.

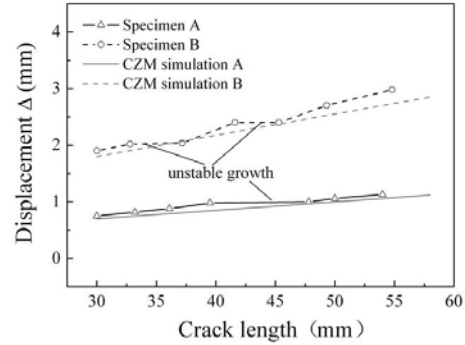


Fig. 10. Numerical and experimental displacement and crack length curves.

The experimental results indicated that for the piezoelectric composite with epoxy resin adhesive, the crack growth was not continuous. Fig. 10 shows that how the crack length varied with load point displacement when unstable growth occurred. The alternating regions of unstable crack growth and stable crack growth can be seen, though the unstable region of the specimen B is not obvious comparing to the specimen A. The crack grows in a static mode, and then undergoes an abrupt transition to unstable crack growth. Fig. 10 also shows the numerically computed curve of the crack length varied with the load point. This curve does not display any significant jumps in the crack length. Results from simulations done by CZM method led to the possibility that certain features about the crack growth were not being captured. It is not appropriate to model the unstable crack growth for the current piezoelectric composite with epoxy resin adhesive in this study. But the model could accommodate the statistical nature of through much experiment by introducing a rate-dependent probability for choosing the unloading portion of the trace separation law.

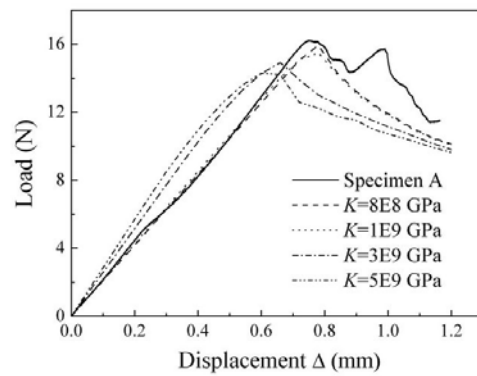


Fig. 11. Effect of initial interface stiffness K on Load - displacement curves.

Some CZM parameters such as the initial interface stiffness, K , can not be measured directly through the

experiments. Therefore, in order to find a reasonable estimation of K various numerical simulations with different K values were compared with experimental results in Fig. 11. Preliminary calculations reveal that the numerical results are more sensitive to the interface stiffness parameter, K , the scope of K is limited. Over the range will cause numerical problems such as converge in interfacial traction of the element or incorrect results. For this reason, K is set to be $1e9$ in all of the simulations, and this choice of K is also able to ensure the convergence of the simulations as well.

5. Conclusions

This paper studies the mixed mode debonding failure in piezoelectric composites following experimental and numerical approaches. The fix-ratio mix-mode (FRMM) loading is a valid testing methodology for evaluating the fracture toughness of piezoelectric composite adhesive interface, this testing configuration proved advantageous due to the absence of machine work needed for the piezoelectric ceramic. The conclusions are as follows:

1. The loading of the FRMM configuration is well described by established fracture mechanics, which should prove more applicable to a variety of piezoelectric composite adhesive structural applications, such as aircrafts, spacecrafts, and even more qualitative piezoelectric ceramic bonding schemes. In addition, from the experimental results, it is shown the strongest interface bond occurred at the adhesive-composite interface. Thus, we expect all failures to occur at the weaker piezoelectric ceramic/adhesive interface.

2. A digital image correlation method for measuring displacement fields with a high speed camera has been coupled with the photoelastic technology to provide a fast and robust way to determine the displacement and strain around the crack tip during the debonding of piezoelectric composite. It was found that, in the current study, the horizontal displacement and strain fields were noisy but of sufficient quality to determine the vertical displacement and strain fields around the adhesive interface. This test provided quantitative evidence of fracture toughness in piezoelectric composite adhesive interface and that is confirmed quantitatively by finite element method.

3. A suggested CZM were employed to simulate the fracture process along the piezoelectric composite adhesive interface. The simulation results reveal that, the CZM was found to be more suitable in describing debonding of weakly bonding interface of piezoelectric composites. And the unstable crack growth of piezoelectric composite adhesive interface could be captured by rate-dependent trace separation law based on statistical method. Such as explore the possibility that the fracture mechanism will be happened assumed to follow a Weibull distribution at any point during loading as follow:

$$P(t) = 1 - \exp\left(-\frac{t}{t_0} \left(\frac{\sigma}{W_0}\right)^m\right) \quad (6)$$

Where t is the time interval over the element which experiences the traction, t_0 is chosen for scaling time, W_0 is a characteristic strength associated with t_0 , σ is the traction of the element, and m is the Weibull modulus which controls the sensitivity of the probability. Such a potential numerical model for the unstable crack growth has been given to provide a possible physical understanding of the unstable crack growth mechanism, a statistical approach may be an appropriate design approach for interface fracture behavior of piezoelectric composites.

Acknowledgements

This work was supported by support of National Natural Science Foundation of China, Grant No. (10872038) and the Fundamental Research Funds for the Central Universities Grant No.DUT11ZD(G)01.

References

- [1] M. Liu, K. J. Hsia, *J Mech Phys Solid*. **51**(5), 921 (2003).
- [2] Q. Li, Y. H. Chen, *Journal of Applied Mechanics*. **75**(1), 011010 (2008).
- [3] Z. C. Ou, Y. H. Chen, *Int J Fracture*. **130**(1), 427 (2004).
- [4] T. B. Du, M. Liu, S. Seghi, K. J. Hsia, *J. Economy, J. K. Shang, Int J Mater Res*. **16**(10), 2885 (2001).
- [5] Y. B. Yan, F. L. Shang, *Int. J. Solids Structure*. **46**(13), 2739 (2009).
- [6] ASTM D-5528, Standard Test Method for Mode I Interlaminar Fracture Toughness of Unidirectional Fiber-Reinforced Polymer Matrix Composites, in *Annual Book of ASTM Standards*, ASTM: West Conshohocken, PA. 2007.
- [7] L. A. Carlsson, J. W. Jr Gillespie, R. B. Pipes, *J. Compos. Mater*. **20**(6), 94 (1986).
- [8] ASTM D-6671, "Standard Test Method for Mixed Mode I-Mode II Interlaminar Fracture Toughness of Unidirectional Fiber Reinforced Polymer Matrix Composites", in *Annual Book of ASTM Standards*, ASTM: West Conshohocken, PA. 2004.
- [8] M. B. Blatz, A. Sadan, M. J. Kern, *Prosthetic Dentistry*, **89** (3), 268 (2003).
- [9] S. Hashemi, A. J. Kinloch, G. Williams, *Mixed-Mode Fracture in Fiber-Polymer Composite Laminates. Composite Materials: Fatigue and Fracture* (Third Volume), ASTM STP 1110, T. K. O'Brien, Ed., American Society for Testing and Materials, Philadelphia, pp. 143-168(1991).
- [10] J. G. Williams, *Journal of Strain Analysis*. **24**(4), 207 (1989).
- [11] J. W. Dally, R. J. Sanford, *Expl Mechanics*. **18**(12), 441 (1978).
- [12] E. E. Gdoutos, G. Papakaliatakis, *Eng Fract Mech*. **16**(2), 177 (1982).
- [13] H. Lu, F. P. Chiang, *Journal of Applied Mechanics*. **1** **60**(1), 93 (1993).
- [14] D. E. Marius, K. K. Sanjeev, *J Eng Mater-T*. **132**(2),

- 021007 (2007).
- [15] D. Xie, S. B. Biggers Jr., *Finite Elem in Anal and Des.* **42**(11), 977 (2006).
- [16] Y. F. Gao, A. F. Bower, *Model and Simul Mater Sc Eng*, **12**(3), 453 (2004).
- [17] A. Hillerborg, M. Modeer, *Cement Concrete Res.* **6**(6), 773 (1976).
- [18] W. G. Knauss, On the steady propagation of a crack in a viscoelastic sheet: experiments and analysis, in: H.H. Kausch, R. Jaffee (Eds.), *Deformation and Fracture of High Polymers*, Plenum Press, New York, 501-541(1973).
- [19] N. Chandra, H. Li, C. Shet, H. Ghonem, *Int. J. Solids Structure.* **39**(10), 2827 (2002).
- [20] T. Ferracin, C. M. Landis, F. Delannay, T. Pardoën, *Int J Solids Structure*, **40**(11), 2889 (2003).
- [21] J. Quinta Da Fonseca, P. M. Mummery, P. J. Withers, *Journal of Microscopy* **218**(1), 9 (2005).
- [22] W. G. Jiang, Stephen R. Hallett, Ben G. Green, Michael R. Wisnom, *Int J Numer Meth Eng.* **69**(9), 1982 (2007).
- [23] C. Sun, M. D. Thouless, A. M. Waas, J. A. Schroeder, P. D. Zavattieri, *Int J Solids Structure.* **45**(17), 4725 (2008).
- [24] A. J. Kinloch, Y. Wang, J. G. Williams, et al. *Compos Sci Technol.* **47**(3), 225(1993).

*Corresponding author: bairx@dlut.edu.cn